Title: Thermal behaviour of Al-rich tobermorite

Running title: Thermal behaviour of Al-rich tobermorite

Plan of the article:

Corresponding author: Elena Bonaccorsi (elena.bonaccorsi@unipi.it)

Computer: PC
OS: Windows
Software: Word
Number of characters (including spaces): 38169

Revision 1

Thermal behaviour of Al-rich tobermorite

CRISTIAN BIAGIONI, ELENA BONACCORSI*, MARCO LEZZERINI, and STEFANO MERLINO[1]

Dipartimento di Scienze della Terra, Università di Pisa, Via S. Maria 53, I-56126 Pisa, Italy

**e-mail address*: elena.bonaccorsi@unipi.it

ABSTRACT

The tobermorite supergroup is composed by a number of calcium-silicate-hydrate (C-S-H) minerals characterized by different hydration states and sub-cell symmetries. Taking into account their basal spacing, closely related to the hydration state, phases having a 14 Å (plombièrite), 11 Å (tobermorite, kenotobermorite, and clinotobermorite), and 9 Å (riversideite) basal spacing have been described. Tobermorite and kenotobermorite belong to the so-called tobermorite group and differ for their thermal behaviour which can be "normal" (the phase shrinks to a 9 Å phase at 300°C) or "anomalous" (the phase preserves its 11 Å basal spacing at 300°C). Specimens of Al-rich tobermorite from Montalto di Castro and Vallerano, Latium, Central Italy, showing a "normal" thermal behaviour, were studied in order to describe the transition from the 11 Å to the 9 Å phase by means of TG-DSC analyses as well as *in-situ* and *ex-situ* X-ray diffraction experiments. TG-DSC analyses showed a continuous mass loss from 100° up to 700°C, with different mass loss gradients between 100° and 300°C and between 300° and 700°C, corresponding to the dehydration of tobermorite and dehydroxylation of "tobermorite 9 Å", respectively. Above 700°C, "tobermorite 9 Å" is replaced by wollastonite. X-ray powder diffraction data were collected at the GILDA beamline of the ESRF, Grenoble, France, from room temperature up to *ca*. 840°C. Tobermorite is completely replaced by the 9 Å phase at *ca*. 300°C, whereas the latter is transformed into wollastonite at *ca*. 700°C. The transition from the 11 Å to the 9 Å phase seems to be favoured by the transient appearance of a clinotobermorite-like compound.

Keywords: Al-rich tobermorite, clinotobermorite, "tobermorite 9 Å", thermal behaviour, "normal" tobermorite, C-S-H.

1. Introduction

The tobermorite supergroup is composed by a series of minerals actively studied for their close structural relationships with C-(A)-S-H [calcium-(aluminium)-silicate-hydrate] gel, the main binding agent of the Portland cement (Taylor, 1964, 1992, 1997; Richardson, 2014). In addition, the hydrothermal formation of tobermorites has been extensively studied during the processing of autoclaved aerated concrete (*e.g.*, Matsui *et al.*, 2011), whereas other potential technological applications have been proposed, *e.g.*, nuclear waste disposal (Shrivastava & Shrivastava, 2000), newsprint recycling (Coleman, 2005), or medical uses (Lin *et al.*, 2007; Coleman *et al.*, 2009).

The tobermorite supergroup is formed by the tobermorite group and the unclassified minerals plombièrite, clinotobermorite, and riversideite (Biagioni *et al.*, 2015). The different species can be distinguished taking into account their basal spacings, corresponding to different hydration states: the greater is the hydration, the wider is the basal spacing. Three different hydration states exist, corresponding to the phases "tobermorite 14 Å" (plombièrite), $Ca_5Si_6O_{16}(OH)_2 \cdot 7H_2O$ (Bonaccorsi *et al.*, 2005), "tobermorite 11 Å" (tobermorite group, clinotobermorite), $Ca_{4+x}Si_6O_{15+2x}(OH)_{2-2x} \cdot 5H_2O$, with $0 < x < 1$ (Merlino *et al.*, 1999, 2001), and "tobermorite 9 Å" (riversideite), $Ca_5Si_6O_{16}(OH)_2$. According to Biagioni *et al.* (2015), two endmember compositions can be distinguished within the tobermorite group, corresponding to kenotobermorite ($x = 0$) and tobermorite ($x = 1$). Each member of the tobermorite supergroup is actually a family of polytypes which can be adequately described through the order-disorder (OD) theory (Dornberger-Schiff, 1956, 1964; Ferraris *et al.*, 2004). Natural and synthetic analogues of these compounds are known. Hereafter, mineral names will be only used when dealing with natural samples, whereas the term "tobermorite" followed by the basal spacing will be used to indicate both natural and synthetic phases.

The members of the tobermorite supergroup ("tobermorites") are structurally characterized by layers of seven-fold coordinated calcium-centred polyhedra, parallel to (001), decorated on both sides by wollastonite-like chains (the so-called *Dreierketten* in Liebau's classification – Liebau, 1985), forming the "complex modules" described in Bonaccorsi & Merlino (2005). Using the cement chemists' terminology, wollastonite chains are formed by "paired" tetrahedra connected by "bridging" tetrahedra. Two kinds of "complex modules" may occur, differing each other in the orientation of the bridging tetrahedra with respect to the paired tetrahedra on the two sides of the calcium polyhedra layers; the occurrence of either one or the other of the two modules results in a monoclinic or orthorhombic sub-cell symmetry.

In the crystal structure of the 11 Å phases (*i.e.* tobermorite, kenotobermorite, and clinotobermorite), the stacking of the complex modules results in the condensation of the wollastonite-like chains into double chains. In the resulting framework, structural cavities occur, hosting "zeolitic" water molecules and in some cases cations (usually calcium, with minor amounts of alkaline metals).

"Tobermorite 11 Å" shows two different thermal behaviours at 300°C. Following the definitions given by Mitsuda & Taylor (1978), "tobermorite 11 Å" is normal if it shrinks to "tobermorite 9 Å" at 300°C; if it does not shrink it is called "anomalous". Mitsuda & Taylor (1978) compared thermal data for thirteen natural specimens of various members of the tobermorite group, observing different thermal behaviours and the existence of a third category of tobermorites, the so-called "mixed", characterized by the coexistence of 11 and 9 Å basal spacings at 300°C. Merlino *et al*. (1999, 2000) put forward an hypothesis explaining the difference between "normal" and "anomalous" thermal behaviour. It seems to be related to the occurrence in "normal tobermorite 11 Å" of additional Ca^{2+} cations hosted in the structural cavities and bonded to three "zeolitic" H_2O molecules, as well as to oxygen atoms of the scaffolding. The loss of these H_2O molecules and the consequent incomplete coordination of Ca^{2+} cations would be the cause for the rearrangement of the structure, through a chain-decondensation and the transformation of "tobermorite 11 Å" into "tobermorite 9 Å", in which Ca^{2+} cations are properly coordinated by the oxygen atoms of the new scaffolding. On the contrary, "anomalous tobermorite 11 Å" does not host additional Ca^{2+} cations in its structural cavities, but only H_2O molecules. Their loss on dehydration does not require any structural shrinking. As discussed by Biagioni *et al*. (2015), members of the tobermorite group form a solid solution between a "zeolitic" Ca-free tobermorite, $Ca_4Si_6O_{15}(OH)_2{\cdot}5H_2O$ (namely kenotobermorite), and a "zeolitic" Ca-bearing tobermorite, $Ca_5Si_6O_{17}{\cdot}5H_2O$ (namely tobermorite), and consequently the distinction between the two thermal behaviours is closely related to the chemistry of the studied samples, intermediate compositions and chemical non-homogeneity probably giving rise to the "mixed" thermal behaviour.

Moreover, at temperature higher than 400°C, "anomalous tobermorite 11 Å" shows two different thermal behaviours, maintaining its 11 Å basal spacing or, on the contrary, transforming into a 10 Å phase (Biagioni *et al*., 2012a, 2012b). Biagioni (2011) suggested a possible role of tetrahedral Al in controlling the thermal behaviour of "anomalous tobermorite 11 Å" at temperature higher than 400°C.

Actually, the role of Al in "tobermorite 11 Å" and C-A-S-H goes well beyond the possible role in the high-temperature thermal behaviour of "anomalous tobermorite 11 Å", because the occurrence of Al significantly improves the chemical stability of concretes with respect of C-S-H

(calcium-silicate-hydrates) (*e.g.*, Jackson *et al.*, 2013). According to several authors, the Al-to-Si substitution takes place at the bridging tetrahedra of the double-wollastonite chains (*e.g.*, Komarneni *et al.*, 1985; Richardson *et al.*, 1993; Yamazaki & Toraya, 2001; Sun *et al.*, 2006; Jackson *et al.*, 2013). Consequently, in agreement with the Loewenstein rule (Loewenstein, 1954), the maximum Al content is 1 atom per formula unit (*apfu*) in order to avoid Al–O–Al bonds.

The aim of this paper is the description of the results of a detailed investigation of the thermal behaviour of specimens of Al-rich tobermorite (Al ~ 1 *apfu*) from two geological occurrences from Latium, Central Italy. A preliminary study of the thermal behaviour of one of these specimens was reported by Merlino *et al.* (2008).

2. Experimental

The studied specimens of Al-rich tobermorite were collected at Montalto di Castro (specimen MDC) and Vallerano (specimen VAL), Latium, Central Italy. They are represented by white compact masses or μm-sized thin acicular to platy crystals (Fig. 1), associated with calcite and ettringite. Tobermorite was first described from Montalto di Castro by Passaglia & Turconi (1982), whereas the occurrence of tobermorite from Vallerano was first reported by Caponera *et al.* (2007).

2.1. Chemical composition

The specimens MDC and VAL were chemically characterized using a Philips XL30 electron microscope equipped with an EDAX energy-dispersive X-ray spectrometer. Analytical conditions were: accelerating voltage 20 kV, beam current 20 nA, beam size 5 μm. Emission lines were calibrated using the following standards: olivine (Mg, Si), albite (Na, Al, Si), orthoclase (K, Al, Si), and diopside (Ca, Mg, Si). In order to check for the reliability of chemical analyses, a crystal of kenotobermorite from the N'Chwaning II mine, Republic of South Africa, $Ca_4Si_6O_{15}(OH)_2 \cdot 5H_2O$, having a well-defined (Ca:Si) atomic ratio was used as an additional reference. Analyses were corrected using the ZAF matrix correction. Chemical analyses, normalized to total = 100 wt %, point to the following compositions (in wt %): SiO_2 48.99, Al_2O_3 7.56, CaO 42.94, K_2O 0.51 for MDC_1; SiO_2 47.73, Al_2O_3 8.68, CaO 42.60, K_2O 0.99 for VAL_1. Both samples are very rich in aluminium; their chemical compositions, based on (Si + Al) = 6 atoms per formula unit (*apfu*), assuming 5 H_2O molecules *pfu*, and adjusting the (OH:O) atomic ratio in order to achieve the electrostatic neutrality, is $(Ca_{4.77}K_{0.07})_{\Sigma 4.84}(Al_{0.92}Si_{5.08})_{\Sigma 6.00}O_{15}(OH_{1.32}O_{0.68}) \cdot 5H_2O$ and $(Ca_{4.72}K_{0.13})_{\Sigma 4.85}(Al_{1.06}Si_{4.94})_{\Sigma 6.00}O_{15}(OH_{1.48}O_{0.52}) \cdot 5H_2O$ for MDC_1 and VAL_1, respectively, approaching the ideal composition $Ca_5AlSi_5O_{16}(OH) \cdot 5H_2O$. These aluminium contents are among

the highest ever reported. Following the recommendations given by Biagioni *et al*. (2015), the specimens from these two occurrences can be classified as tobermorite.

2.2. Thermo-gravimetric analysis

About 25 mg of powdered tobermorite from the two localities, samples MDC_2 and VAL_2 respectively, were used for the data collection. The thermal analyses were performed by means of a simultaneous TG-DSC-QMS equipment (Netzsch STA 449C Jupiter). The experimental conditions were: *a*) continuous heating from room temperature (20°C) up to 1000°C, at a constant heating rate of 10°C·min^{-1}; *b*) inert-gas (N_2) dynamic atmosphere (30 ml·min^{-1}); *c*) alumina, top-opened crucible; *d*) no pre-heating treatment of the samples, in order to prevent a possible loss of weakly bonded H_2O molecules. A small amount of powder sample MDC_3 (about 10 mg) was additionally heated up to 300°C, using the same heating rate of the previous experiments, in order to study the heating product at this temperature.

2.3. X-ray powder diffraction study

The products of the thermo-gravimetric analyses MDC_2, MDC_3 and VAL_2 were identified by means of X-ray powder diffraction (XRPD) using a Bragg-Brentano geometry and Ni-filtered Cu *K*α radiation, under the following experimental conditions: scan range 4 - 65° in 2θ, scan step 0.02°, scan time 2 s.

For the Montalto di Castro specimen *in-situ* time-resolved X-ray powder diffraction (TR-XRD) patterns were collected at the GILDA (General Italian Line for Diffraction and Absorption) beamline, at the European Synchrotron Radiation Facility, Grenoble, France. A 0.5 mm amorphous silica capillary was filled with the powder MDC_4, and the data were collected in the Debye-Scherrer transmission geometry, using the experimental apparatus described in Meneghini *et al*. (2001). The two slits in front of the image plate (IP) allowed the selection of a vertical slice of the Debye rings generated by the diffracting powder, which rotated about the φ axis while the recording IP support was linearly translated behind the slits, at constant speed. Consequently, the diffraction pattern was recorded as a function of time and sample treatment. This experimental setup allowed the collection of a continuous diffraction pattern while the sample was heated by a hot air-blower. Sample to detector distance and detector tilt were carefully calibrated against LaB_6 (SRM 660a). The calibration of the heating apparatus was performed by measuring accurate Rietveld-refined lattice parameters of standards with known thermal expansion coefficient (Meneghini *et al*., 2001). The data, stored in the latent image, were recovered and digitized using a Fuji BAS-2500 laser scanner with a 100 × 100 μm^2 pixel size and a dynamic range of 16 bit/pixel. The digitized images were integrated using the FIT2D (Hammersley *et al*., 1996) software to have intensity *versus* 2θ diffraction patterns.

The sample MDC_4 was heated from room temperature (25°C) up to 843°C, with a heating rate of *ca*. 3.5°C/min. Initially, the powder sample was maintained at 25°C for 15 minutes, then heated up to 843°C. Finally, it was maintained at the final temperature for 15 minutes. The radiation wavelength was set at $\lambda = 0.78348$ Å; the measured 2θ ranges between 1° and 45°.

The cell parameters were refined using the GSAS program (Larson & Von Dreele, 1994) with the EXPGUI graphical user interface (Toby, 2001). The refinements of the unit-cell parameters were carried out by means of the Le Bail method (Le Bail *et al*., 1988). The background was fitted with a shifted-Chebyshev function, using a number of terms ranging from 10 to 16; the profile shape was modelled by Pseudo-Voigt functions, refining the Gaussian parameters GW, the Lorentzian parameters LX and LY, and the asymmetry of the peak profiles.

3. Results and discussion

3.1. Chemical data and aluminium content in minerals of the tobermorite supergroup

Minerals belonging to the tobermorite supergroup have a wide range of aluminous compositions. Figure 2 shows the chemical variability of the 11 Å phases (tobermorite, kenotobermorite, and clinotobermorite) using data available in literature. Only those analyses recalculated on the basis of (Si + Al) = 6 *apfu* resulting in Ca ≥ *ca*. 4 *apfu* and $4 \leq \Sigma(Ca+Na+K) \leq 5$ *apfu* have been considered. Data are reported in Biagioni (2011). Three groups can be distinguished: *i*) Al-free "tobermorites", *ii*) Al-bearing "tobermorites", and *iii*) Al-rich "tobermorites". The first class is uncommon and is represented by specimens of tobermorite from Castle Hill, Ayrshire, Scotland, UK (Webb, 1971), tobermorite and kenotobermorite from Cornet Hill, Apuseni Mountains, Romania (Marincea *et al*., 2001), kenotobermorite from N'Chwaning II mine, Kalahari Manganese Field, South Africa (Merlino *et al*., 2001; Biagioni *et al*., 2012a), and clinotobermorite from Wessels mine, Kalahari Manganese Field, South Africa (Hoffmann & Armbruster, 1997; Merlino *et al*., 2000; Biagioni, 2011) and Bazhenovskoe, Urals, Russia (Biagioni, 2011). In addition, clinotobermorite from its type-locality, Fuka, is very poor in Al (0.05 *apfu* – Henmi & Kusachi, 1992). The second group (Al-bearing "tobermorites") contains the majority of the tobermorite occurrences (both kenotobermorite and tobermorite). On the contrary, Al-rich "tobermorites" are very rare and up to now are represented exclusively by three occurrences: Montalto di Castro and Vallerano, Latium, Italy; and the K-rich tobermorite from Höwenegg, Hegau, Germany (Walenta, 1974; Biagioni, 2011).

The substitution of Si^{4+} by Al^{3+} should be balanced according to two possible mechanisms: *i*) $Si^{4+} + \square = Al^{3+} + (Na,K)^{+}$, and *ii*) $Si^{4+} + O^{2-} = Al^{3+} + (OH)^{-}$. In "tobermorites" having partially occupied interlayers, the mechanism *i*) is possible, whereas the mechanism *ii*) could be

hypothesized in phases approaching the endmember composition $Ca_5Si_6O_{17}\cdot 5H_2O$. In the latter case, corresponding to the chemistry of tobermorite samples from Latium, the introduction of Al^{3+} should be coupled with protonation of an oxygen atom. This second substitution mechanism agrees with the increase in the silanol binding capacity reported in C-A-S-H having low Ca/Si ratios (Richardson & Groves, 1993; Taylor *et al*., 2010).

3.2. Thermo-gravimetric data

Figure 3 shows thermo-gravimetric (TG) and differential scanning calorimetry (DSC) curves collected on the samples MDC_2 (Fig. 3a) and VAL_2 (Fig. 3b). In agreement with the very similar chemical composition of these two specimens, the TG and DSC curves are very similar. For this reason, in the following we shall refer only to the sample MDC_2.

Passaglia & Turconi (1982) described the close association of tobermorite with ettringite; this calcium-aluminium-sulphate hydrate mineral was also observed in the powder sample used for the *in-situ* X-ray diffraction study (sample MDC_4). Consequently, in order to verify its occurrence, a preliminary X-ray powder diffraction (XRPD) pattern was collected on the same sample MDC_2 used for TG-DSC analysis. The XRPD pattern did not show diffraction effects related to the presence of ettringite; therefore, if it is present, its amount is probably less than 5 wt%.

The TG curve shows a continuous mass loss from about 100°C up to about 700°C. This temperature range can be divided into two intervals, characterized by different gradients of mass loss. Between 100°C and 250°C, there is an important mass loss, associated with an endothermic hump in the DSC curve. It corresponds to a mass loss of about 11 wt %, assuming a mass loss of about 1 wt % between room temperature and 100°C. This very first process could be due to the loss of humidity adsorbed on the surface of the powder grains and/or to the incipient dehydration of the possible low amount of ettringite eventually occurring. As stated above, if present, ettringite could represent less than 5 wt % in sample MDC_2; however, owing to its very high H_2O content, this low amount of ettringite could contribute to the mass loss, in particular within 150°C. It is known from XRPD (see below) that at *ca*. 300°C tobermorite is replaced by "tobermorite 9 Å". The chemical composition of the latter should be $Ca_5AlSi_5O_{15}(OH)_3$ in the specimen MDC. Therefore, the theoretical mass loss between room temperature and 300°C should be about 10 wt %, in good agreement with the observed value. The small difference (about 1 wt %) may be due, as it was already stated above, to a very limited amount of admixed ettringite or/and to adsorbed humidity. A mass loss of about 10 wt % corresponds to the loss of four H_2O molecules *pfu*, in agreement with previous studies by Shaw *et al*. (2000) and Biagioni *et al*. (2012a). The dehydration process of Al-rich tobermorite may be expressed as

$$Ca_5(AlSi_5)O_{16}(OH)\cdot 5H_2O - 4H_2O \rightarrow Ca_5(AlSi_5)O_{15}(OH)_3$$

Between 250°C and 700°C, there is a constant mass loss of about 5 wt %, probably corresponding to the dehydroxylation of "tobermorite 9 Å". At 700°C, the DSC curve shows an exothermic hump, probably related to the crystallization of wollastonite, as revealed by XRPD on the final products of the heating process.

3.3. X-ray powder diffraction data

The heating-induced transformation of Al-rich tobermorite was studied through two different X-ray diffraction experiments:

i) identification of the products of the thermo-gravimetric analyses;

ii) *in-situ* TR-XRD.

X-ray powder diffraction patterns collected on samples MDC_2 and VAL_2 heated up to 1000°C during the thermo-gravimetric analyses indicated that the final product of the heating process is represented by wollastonite. In addition, the heating of the sample MDC_3 up to 300°C resulted in the formation of a phase characterized by a 9.6 Å basal spacing (hereafter called "tobermorite 9 Å").

The powder sample MDC_4 was used for the collection of *in-situ* TR–XRD (Fig. 4). The unit-cell parameters of tobermorite from Montalto di Castro, refined at room temperature, are a = 6.7267(5), b = 7.3949(3), c = 22.985(1) Å, β = 123.302(5)°, space group $B11m$. The c parameter is larger than those observed in other "tobermorites" (*e.g.*, c = 22.487(4) Å in kenotobermorite from N'Chwaning II mine, South Africa; c = 22.680(4) Å in tobermorite from Urals – Merlino *et al*., 2001). The larger interlayer spacing is related to the Al-to-Si substitution, in agreement with Diamond *et al*. (1966) and Jackson *et al*. (2013), as the Al–O distances are *ca*. 8-10% longer than Si–O bond lengths.

The processes taking place in the powder sample were rather complex. At room temperature, the sample MDC_4 was a mixture of Al-rich tobermorite and ettringite. This latter phase disappeared before 130°C, becoming apparently amorphous. Al-rich tobermorite maintained its 11 Å basal spacing up to *ca*. 240°C; at this temperature, "tobermorite 9 Å" began to appear. As it will be discussed later, in the temperature range between 180°C and 240°C some small diffraction peaks pointed to the possible formation of a clinotobermorite-like phase.

The polymorphs of the 11 Å phase belonging to the tobermorite supergroup (tobermorite and kenotobermorite, belonging to the tobermorite group, and clinotobermorite) could be identified on the basis of some "family reflections". It seems proper to stress that "family reflections" in the tobermorite group are those reflections corresponding to even k indices, reflections which have the same positions and intensities in all the structures of the family (ordered and disordered). Taking into account this class of reflections, tobermorite and kenotobermorite could be distinguished from

clinotobermorite. In particular, considering the "family cells", *i.e.* the cells defined by considering only the "family reflections", the distinction could be made using the following ranges of d_{hkl}: *i*) in the d_{hkl} range between 5 and 6 Å ($7 \leq 2\theta \leq 10°$), tobermorite showed only the 101 reflection (d_{101} = 5.45 Å), whereas clinotobermorite had two weaker reflections, at 5.59 and 5.28 Å; *ii*) in the d_{hkl} range between 2.95 and 3.10 Å ($14 \leq 2\theta \leq 16°$), the X-ray diffraction pattern of tobermorite was characterized by two reflections at 3.08 and 2.978 Å, whereas clinotobermorite had two reflections at 3.07 and 3.01 Å, with the latter stronger than the former; and *iii*) the 215 reflection of clinotobermorite, at d_{215} = 1.92 Å, occurred in a d_{hkl} range in which tobermorite did not show any reflection. Figure 5 shows these three 2θ(°) ranges, corresponding to the diagnostic d_{hkl} intervals, and illustrates their changes as a function of increasing temperature. In the $7 \leq 2\theta \leq 10°$ range, the 101 reflection (d_{101} = 5.45 Å at room temperature) of tobermorite decreased its intensity from 128°C to 238°C and it became larger, possibly owing to the contribution of two weak reflections at lower and higher 2θ angles, potentially corresponding to the reflections at 5.59 and 5.28 Å typical of clinotobermorite. In the $14 \leq 2\theta \leq 16°$ range, the two reflections at 3.08 and 2.98 Å became progressively weaker, owing to the appearance, at temperatures higher than 238°C, of the 3.03 Å reflections of "tobermorite 9 Å". Finally, in the $22 \leq 2\theta \leq 25°$ range, it was particularly clear how the reflection at d_{hkl} = 1.92 Å was absent at room temperature, appeared around 180°C, reached its maximum intensity at *ca*. 210°C, then disappearing. These data can be interpreted as the transient formation of a clinotobermorite-like phase during the transition from Al-rich tobermorite to "tobermorite 9 Å".

Tobermorite completely disappeared before *ca*. 293°C; above this temperature, the only phase occurring in the powder sample was represented by "tobermorite 9 Å". Figure 6 shows the variation of the unit-cell parameters of tobermorite during the TR–XRD experiment, normalized to their initial values. The *a*, *b*, and *c* unit-cell parameters (Fig. 6a) of Al-rich tobermorite were rather constant up to ca. 180°C; at this temperature there was an increase in the length of the a axis, whereas the other two axes slightly shortened. At *ca*. 230°C, a strong drop in the *b* parameter was observed, whereas the *c* periodicity increase. Figure 6b shows the relative variations of the unit-cell volume *V*, normalized to the value at room temperature V_0. At temperature higher than 150°C, the unit-cell volume tends to decrease up to 200°C. Then, between 200° and ca. 230°C, the cell volume expanded. Finally, an important drop in the unit-cell volume was observed, related to the first appearance of "tobermorite 9 Å". Above this temperature, only the "family cells" of "tobermorite 11 Å" could be observed. The behaviour of the unit-cell parameters of Al-rich tobermorite as a function of temperature can be compared with those reported for "anomalous" tobermorite by Shaw *et al*. (2000) and Biagioni *et al*. (2012a) in the same temperature range. According to these authors,

a decrease in the *a* parameter was observed up to *ca*. 200°C, interpreted as due to the loss of molecular H_2O; this change seems to be less important in Al-rich tobermorite. Maybe, the occurrence of "zeolitic" calcium cations bonded to these H_2O molecules in the studied specimen could inhibit their loss. The increase in the *c* parameter of Al-rich tobermorite from Montalto di Castro could be compared with a similar but more progressive increase reported in "anomalous" tobermorite from the N'Chwaning II mine up to 450°C by Biagioni *et al*. (2012a).

Figure 7 illustrates the comparison between *c* parameters in Al-rich tobermorite and its partly dehydrated product, "tobermorite 9 Å". No significant changes of the *c* periodicity of the latter have been observed up to its transformation into wollastonite occurring at *ca*. 800°C. This behaviour was different from that shown by "tobermorite 9 Å" obtained through the dehydration of plombièrite and reported by various authors (Farmer *et al*., 1966; Mitsuda & Taylor, 1978; Biagioni *et al*., 2013). In fact, a progressive shift of the basal reflection of the 9 Å phase up to values around 10 Å was observed, indicating a progressive expansion upon heating.

3.4. The transition from "tobermorite 11 Å" to "tobermorite 9 Å"

The transition from "tobermorite 11 Å" to "tobermorite 9 Å" upon heating ("normal" behaviour according to Mitsuda & Taylor, 1978) was firstly described by McConnell (1954), using crystals from Ballycraigy, County Antrim, Northern Ireland, UK. Taylor (1959) studied the transformation tobermorite → "tobermorite 9 Å" → wollastonite, highlighting the topotactic nature of these transitions (Lotgering, 1959; Günter & Oswald, 1975) and proposing a structural model for "tobermorite 9 Å".

A "normal" behaviour was also shown by clinotobermorite; using crystals of this mineral from the Wessels mine, Kalahari Manganese Field, South Africa, Merlino *et al*. (2000) solved its real crystal structure as well as that of its dehydrated product, namely "clinotobermorite 9 Å", topotactically obtained from the former at 300°C. On the contrary, up to now, an accurate solution of the real crystal structure of "tobermorite 9 Å" was not possible. The reason could be sought in the possible mechanism favouring the transition from the 11 to the 9 Å phases. As suggested by the in-*situ* TR–XRD study of Al-rich tobermorite from Montalto di Castro, a clinotobermorite-like phase seems to form as an intermediate compound between "tobermorite 11 Å" and its partly dehydrated product "tobermorite 9 Å". As a matter of fact, clinotobermorite has a double silicate chain arrangement favouring the crystal structure shrinkage after the chain-decondensation.

As hypothesized by Biagioni *et al*. (2012b) for the transformation "tobermorite 11 Å" → "tobermorite 10 Å", during the first step of dehydration (T < 300°C), an important H^+ diffusion in the crystal structure of tobermorite could take place. The H^+ ions could act as catalysts for the migration of Si^{4+} ions, favouring the transformation of the silicate chains from a tobermorite-like to

a clinotobermorite-like configuration. Then, the shrinkage of the structure could take place through the break of the Si–O–Si bond at the bridging tetrahedra, with a relative shift of a "complex module" with respect to the others. In agreement with Merlino *et al*. (1999, 2000), the chain decondensation and the transition from "tobermorite 11 Å" to "tobermorite 9 Å" allows a proper coordination of Ca^{2+} cations hosted with the structural cavities, compensating for the loss after dehydration of the H_2O molecules forming their coordination shell.

It is important to stress that the transition "tobermorite"–"clinotobermorite" is the main cause of the high structural disorder observed along c. In fact, in successive layers, the shift of the complex modules can take place in different directions. On the contrary, the dehydration of natural clinotobermorite should induce only the break of the Si–O–Si bonds of the bridging tetrahedra, favouring the crystallization of a relatively ordered 9 Å phase. This could explain why for "clinotobermorite 9 Å" it was possible to solve and refine not only the family structure but also the crystal structures of both its two MDO polytypes (Merlino *et al*., 2000), whereas for "tobermorite 9 Å" only broad family reflections were observed, allowing only for a rough comparison between the structural model and the powder diffraction pattern.

4. Conclusions

The observed normal thermal behaviour of Al-rich tobermorite, ideally $Ca_5AlSi_5O_{16}(OH)\cdot 5H_2O$, is in agreement with the hypothesis of Merlino *et al*. (1999, 2000). The transition from the 11 Å to the 9 Å phase occurs between 240° and 300°C and it seems to be preceded by the occurrence of a clinotobermorite-like phase in the temperature range 180°-240°C. The transient occurrence of a clinotobermorite-like phase was reported also by Biagioni *et al*. (2012a) during the transformation from "tobermorite 11 Å" (actually kenotobermorite) and "tobermorite 10 Å". In the type description of natural clinotobermorite Henmi & Kusachi (1992) proposed that this mineral could be a low-temperature polymorph of tobermorite; on the contrary, recent data suggest that clinotobermorite could be a relatively high-T phase. Further studies are mandatory to determine the actual relationships between natural clinotobermorite and thermal-obtained clinotobermorite.

"Tobermorite 9 Å" first crystallizes at ca. 240°C and completely replaces the 11 Å phase at 300°C. Then, it preserves its basal spacing up to its transformation to wollastonite, at ca. 700°C. On the basis of these data, "tobermorite 9 Å" obtained from the partial dehydration of the 11 Å phase seems to be different from the 9 Å compound obtained starting from plombièrite ("tobermorite 14 Å"). Indeed, the latter expands its basal spacing upon heating, up to ca. 10 Å (Farmer *et al*., 1966; Biagioni *et al*., 2013).

Whereas the different thermal behaviours of "tobermorites" up to 300°C seems to be predictable on the basis of the occurrence of "zeolitic" calcium cations within the structural cavities (Merlino *et al*., 1999, 2000), the complex structural transformations at temperatures higher than 300°C are not yet fully understood, and further studies on specimens having different chemistry are mandatory in order to propose a general scheme of the transformations affecting these C-S-H phases upon heating.

Acknowledgments

This work was supported by MIUR (Ministero dell'Istruzione, dell'Università e della Riceca) through grants to the national project PRIN 2009 "Structures, microstructure and properties of minerals". The specimen of tobermorite from Vallerano was kindly provided by the mineral collector Edgardo Signoretti. We are grateful to professor Gilberto Artioli, who kindly collected at ESRF the TR-XRD data discussed in this paper . We thank the anonymous reviewers for their constructive comments, which helped us in improving the paper.

Our thanks are due to professor Thomas Armbruster, who collaborated with us in some of the previous structural studies of kenotobermorite and clinotobermorite, providing also some valuable specimens of these complicated minerals. We gratefully dedicate this piece of work to him, in occasion of his retirement.

References

Biagioni, C. (2011): I silicati idrati di calcio: assetto strutturale e comportamento termico. Ph.D. Thesis, Pisa University, 300 p.

Biagioni, C., Bonaccorsi, E., Lezzerini, M., Merlini, M., Merlino, S. (2012a): Thermal behaviour of tobermorite from N'Chwaning II mine (Kalahari Manganese Field, Republic of South Africa). I. Thermo-gravimetric and X-ray diffraction studies. *Eur. J. Mineral.*, **24**, 981–989.

Biagioni, C., Bonaccorsi, E., Merlino, S., Bersani, D., Forte, C. (2012b): Thermal behaviour of tobermorite from N'Chwaning II mine (Kalahari Manganese Field, Republic of South Africa). II. Crystallographic and spectroscopic study of tobermorite 10 Å. *Eur. J. Mineral.*, **24**, 991–1004.

Biagioni, C., Bonaccorsi, E., Merlino, S., Bersani, D. (2013): New data on the thermal behavior of 14 Å tobermorite. *Cem. Concr. Res*., **49**, 48–54.

Biagioni, C., Merlino, S., Bonaccorsi, E. (2015): The tobermorite supergroup: a new nomenclature. *Mineral. Mag*., **79**, 485–495.

Bonaccorsi, E. & Merlino, S. (2005): Modular microporous minerals: cancrinite-davyne group and C-S-H phases. *Rev. Mineral. Geochem.*, **57**, 241–290.

Bonaccorsi, E., Merlino, S., Kampf, A. (2005): The crystal structure of tobermorite 14 Å (plombierite), a C-S-H phase. *J. Amer. Ceram. Soc.*, **88**, 505–512.

Caponera, I., Fiori, S., Pucci, R., Signoretti, E. (2007): I minerali dei Colli Albani. Un aggiornamento sugli ultimi dieci anni di ricerche. *Riv. Mineral. Ital.*, **31**, 74–91.

Coleman, N.J. (2005): Synthesis, structure and ion exchange properties of 11 Å tobermorite from newsprint recycling residue. *Mat. Res. Bull.*, **40**, 2000–2013.

Coleman, N.J., Bishop, A.H., Booth, S.E., Nicholson, J.W. (2009): Ag^{+}- and Zn^{2+}-exchange kinetics and antimicrobial properties of 11 Å tobermorites. *J. Eur. Ceram. Soc.*, **29**, 1109–1117.

Diamond, S., White, J.L., Dolch, W.L. (1966): Effects of isomorphous substitution in hydrothermally-synthesized tobermorite. *Am. Mineral*., **51**, 388–401.

Dornberger Schiff K. (1956): On the order-disorder (OD-structures), Acta Cryst 9 (1956) 593-601.

Dornberger Schiff K. (1964): Grundzüge einer Theorie von OD-Strukturen aus Schichten, Abhandlungen der Deutschen Akademie der Wissenschaften zu Berlin, Klasse für Chemie, Geologie und Biologie 3 (1964) 1-107**.**

Farmer, V.C., Jeevaratnam, J., Speakman, K., Taylor, H.F.W. (1966): Thermal decomposition of 14 Å tobermorite from Crestmore. *in* "Proceedings of Symposium "Structure of Portland Cement Paste and Concrete", Special Report **90**", Highway Research Board, Washington, DC, 291–299.

Ferraris, G., Makovicky, E., Merlino, S. (2004): Crystallography of Modular Materials. Oxford University Press.

Günter, J.R. & Oswald, H.R. (1975): Attempt to a systematic classification of topotactic reactions. *Bull. Inst. Chem. Res*., **53**, 249–255.

Hammersley, A.P., Svensson, S.O., Hanfland, M., Fitch, A.N., Häusermann, D. (1996): Two-dimensional detector software: from real detector to idealized image or two-theta scan. *High Press. Res.*, **14**, 235–248.

Henmi, C. & Kusachi, I. (1992): Clinotobermorite, $Ca_5Si_6(O,OH)_{18}\cdot 5H_2O$, a new mineral from Fuka, Okayama Prefecture, Japan. *Mineral. Mag*., **56**, 353–358.

Hoffmann, C. & Armbruster, T. (1997): Clinotobermorite, $Ca5[Si_3O_8(OH)]_2\cdot 4H_2O$ – $Ca_5[Si_6O_{17}]\cdot 5H_2O$, a natural C-S-H(I) type cement mineral: determination of the substructure. *Z. Kristallogr*., **212**, 864–873.

463 Jackson, M.D., Chae, S.R., Mulcahy, S.R., Meral, C., Taylor, R., Li, P., Emwas, A.-H., Moon, J.,
464 Yoon, S., Vola, G., Wenk, H.-R., Monteiro, P.J.M. (2013): Unlocking the secrets of Al-
465 tobermorite in Roman seawater concrete. *Am. Mineral.*, **98**, 1669–1687.
466 Komarneni, S., Roy, R., Roy, D.M., Fyfe, C.A., Kennedy, G.J., Bothner-By, A.A., Dadok, J.,
467 Chesnick, A.S. (1985): ^{27}Al and ^{29}Si magic angle spinning nuclear magnetic resonance
468 spectroscopy of Al-substituted tobermorites. *J. Mat. Sci.*, **20**, 4209–4214.
469 Larson, A.C. & Von Dreele, R.B. (1994): General Structure Analysis System (GSAS). Los Alamos
470 National Laboratory Report LAUR 86–748.
471 Le Bail, A., Duroy, H., Fourquet, J.L. (1988): *Ab initio* structure determination of $LiSbWO_6$ by X-
472 ray powder diffraction. *Mat. Res. Bull.*, **23**, 447–452.
473 Liebau, F. (1985): *Structural Chemistry of Silicates – Structures, Bonding, and Classification.*
474 Springer-Verlag, Berlin.
475 Lin, K., Chang, J., Cheng, R. (2007): *In vitro* hydroxyapatite forming ability and dissolution of
476 tobermorite nanofibers. *Acta Biomater.*, **3**, 271–276.
477 Loewenstein, W. (1954): The distribution of aluminum in the tetrahedra of silicates and aluminates.
478 *Am. Mineral.*, **39**, 92–96.
479 Lotgering, F.K. (1959): Topotactical reactions with ferromagnetic oxides having hexagonal crystal
480 structures. *J. Inorg. Nucl. Chem*., **9**, 113.
481 Marincea, S., Bilal, E., Verkaeren, J., Pascal, M., Fonteilles, M. (2001): Superposed parageneses in
482 the spurrite-, tilleyite-, and gehlenite-bearing skarns from Cornet Hill, Apuseni Mountains,
483 Romania. *Can. Mineral.*, **39**, 1435–1453.
484 Matsui, K., Kikuma, J., Tsunashima, M., Ishikawa, T., Matsuno, S., Ogawa, A., Sato, M. (2011): *In*
485 *situ* time-resolved X-ray diffraction of tobermorite formation in autoclaved aerated concrete:
486 influence of silica source reactivity and Al addition. *Cem. Concr. Res*., **41**, 510–519.
487 McConnell, J.D.C. (1954): The hydrated calcium silicates riversideite, tobermorite, and plombierite.
488 *Mineral. Mag*., **30**, 293–305.
489 Meneghini, C., Artioli, G., Balerna, A., Gualtieri, A.F., Norby, P., Mobilio, S. (2001): Multipurpose
490 imaging-plate camera for in-situ powder XRD at the GILDA beamline. *J. Synchr. Rad.*, **8**,
491 1162–1166.
492 Merlino, S., Bonaccorsi, E., Armbruster, T. (1999): Tobermorites: Their real structure and order-
493 disorder (OD) character. *Am. Mineral.*, **84**, 1613–1621.
494 Merlino, S., Bonaccorsi, E., Armbruster, T. (2000): The real structure of clinotobermorite and
495 tobermorite 9 Å: OD character, polytypes, and structural relationship. *Eur. J. Mineral*., **12**,
496 411–429.

497 Merlino, S., Bonaccorsi, E., Armbruster, T. (2001): The real structure of tobermorite 11 Å: normal
498 and anomalous forms, OD character and polytypic modifications. *Eur. J. Mineral.*, **13**, 577–
499 590.
500 Merlino, S., Bonaccorsi, E., Merlini, M., Marchetti, F., Garra, W. (2008): Tobermorite 11 Å and its
501 synthetic counterparts: structural relationships and thermal behaviour. *In* S. Krivovichev ed.,
502 "Minerals as advanced materials. I", 37–44. Springer, Berlin
503 Mitsuda, T. & Taylor, H.F.W. (1978): Normal and anomalous tobermorites. *Mineral. Mag.*, **42**,
504 229–235.
505 Passaglia, E. & Turconi, B. (1982): Silicati ed altri minerali di Montalto di Castro (Viterbo). *Riv.*
506 *Mineral. Ital.*, **6**, 97–109.
507 Richardson, I.G. (2014): Model structures for C-(A)-S-H(I). *Acta Crystallogr*., **B70**, 903–923.
508 Richardson, I.G. & Groves, G.W. (1993): The incorporation of minor and trace elements into
509 calcium silicate hydrate (C-S-H) gel in hardened cement pastes. *Cem. Concr. Res*., **23**, 131–
510 138.
511 Richardson, I.G., Brough, A.R., Brydson, R., Groves, G.W., Dobson, C.M. (1993): The location of
512 aluminum in substituted calcium silicate hydrate (C-S-H) gels as determined by ^{29}Si and ^{27}Al
513 NMR and EELS. *J. Am. Ceram. Soc.*, **76**, 2285–2288.
514 Shaw, S., Henderson, C.M.B., Komanschek, B.U. (2000): Dehydration/recrystallization
515 mechanism, energetics, and kinetics of hydrated calcium silicate minerals: an in situ
516 TGA/DSC and synchrotron radiation SAXS/WAXS study. *Chem. Geol.*, **167**, 141–159.
517 Shrivastava, O.P. & Shrivastava, R. (2000): Cation exchange applications of synthetic tobermorite
518 for the immobilization and solidification of cesium and strontium in cement matrix. *Bull.*
519 *Mat. Sci.*, **23**, 515–520.
520 Sun, G.K., Young, J.F., Kirkpatrick, R.J. (2006): The role of Al in C–S–H: NMR, XRD, and
521 compositional results from precipitated samples. *Cem. Concr. Res.*, **36**, 18-29.
522 Taylor, H.F.W. (1953): Hydrated calcium silicates. Part V. The water content of calcium silicate
523 hydrate (I). *J. Chem. Soc.*, **12**, 163–171.
524 Taylor, H.F.W. (1959): The dehydration of tobermorite. *Proc. 6th Nat. Conf. Clays and Clay*
525 *Minerals*, Pergamon Press, 101–109.
526 Taylor, H.F.W. (1964): The calcium silicate hydrates. *in* "The Chemistry of Cements", H.F.W.
527 Taylor, ed., Academic Press, London, 167–232.
528 Taylor, H.F.W. (1992): Tobermorite, jennite, and cement gel. *Z. Kristallogr.*, **202**, 41–50.
529 Taylor, H.F.W. (1997): Cement Chemistry. 2nd edition. Thomas Telford Publishing, London.

530 Taylor, R., Richardson, I.G. & Brydson, R.M.D. (2010): Composition and microstructure of 20-
531 year-old ordinary Portland cement-ground granulated blast-furnace slag blends containing 0
532 to 100% slag. *Cem. Concr. Res*., **40**, 971–983.
533 Toby, B.H. (2001): EXPGUI, a graphical user interface for GSAS. *J. Appl. Crystallogr*., **34**, 210–
534 213.
535 Walenta, K. (1974): Zeolithparagenesen aus dem Melilith-Nephelinit des Höwenegg im Hegaus.
536 *Aufschluss*, **25**, 613–626.
537 Webb, A.B.S.J. (1971): Tobermorite from Castle Hill near Kilbirnie, Ayrshire. *Mineral. Mag*., **38**,
538 253.
539 Yamazaki, S. & Toraya, H. (2001): Determination of positions of zeolitic calcium atoms and water
540 molecules in hydrothermally formed alumina-substituted tobermorite-1.1 nm using
541 synchrotron radiation powder diffraction data. *J. Am. Ceram. Soc.,* **84**, 2685–2690.
542

543 **Figure 1** – Globular aggregates of thin platy crystals of tobermorite associated with calcite.
544 Vallerano, Latium, Italy.

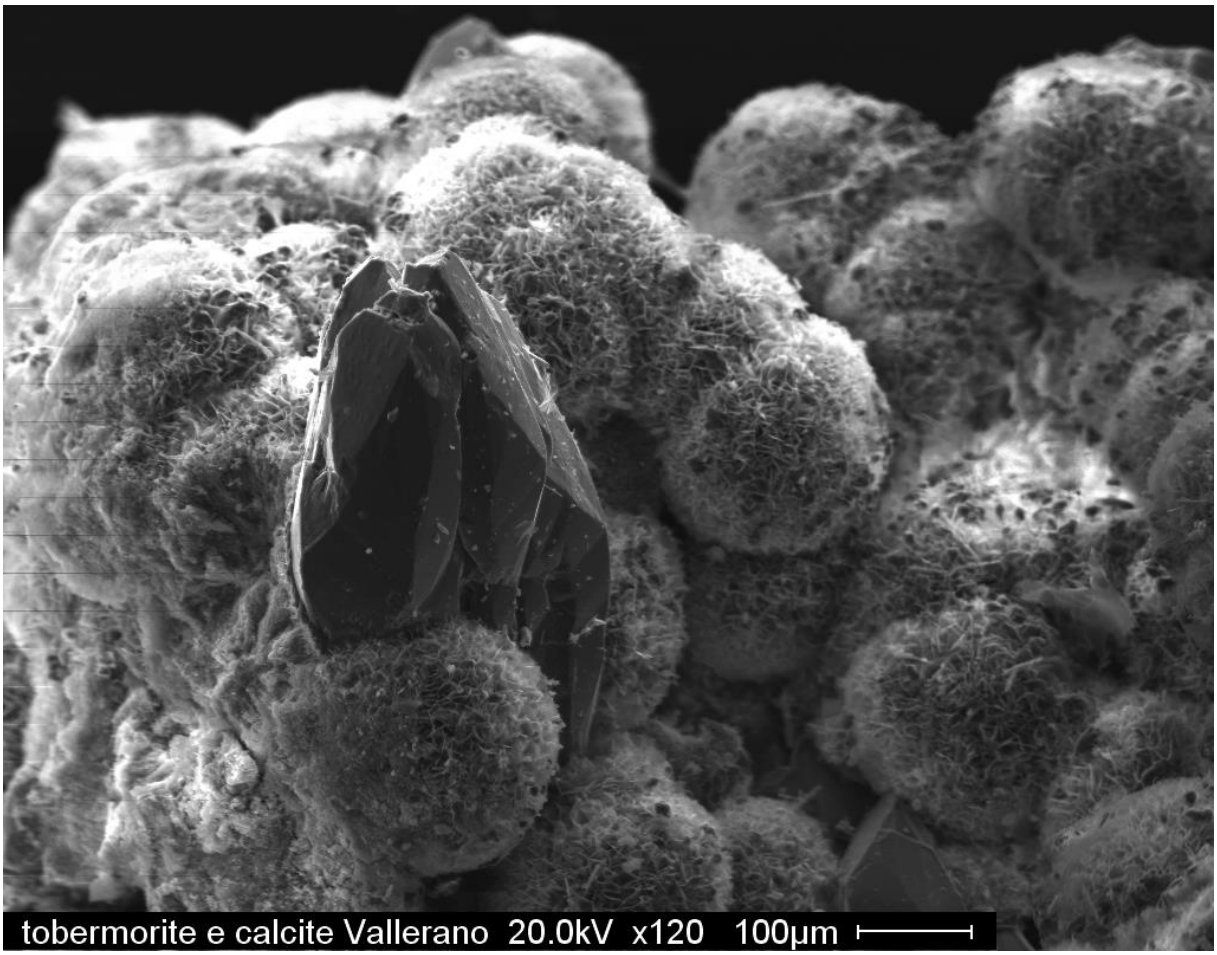

545
546

547 **Figure 2** – Chemical variability in natural 11 Å members of the tobermorite supergroup.

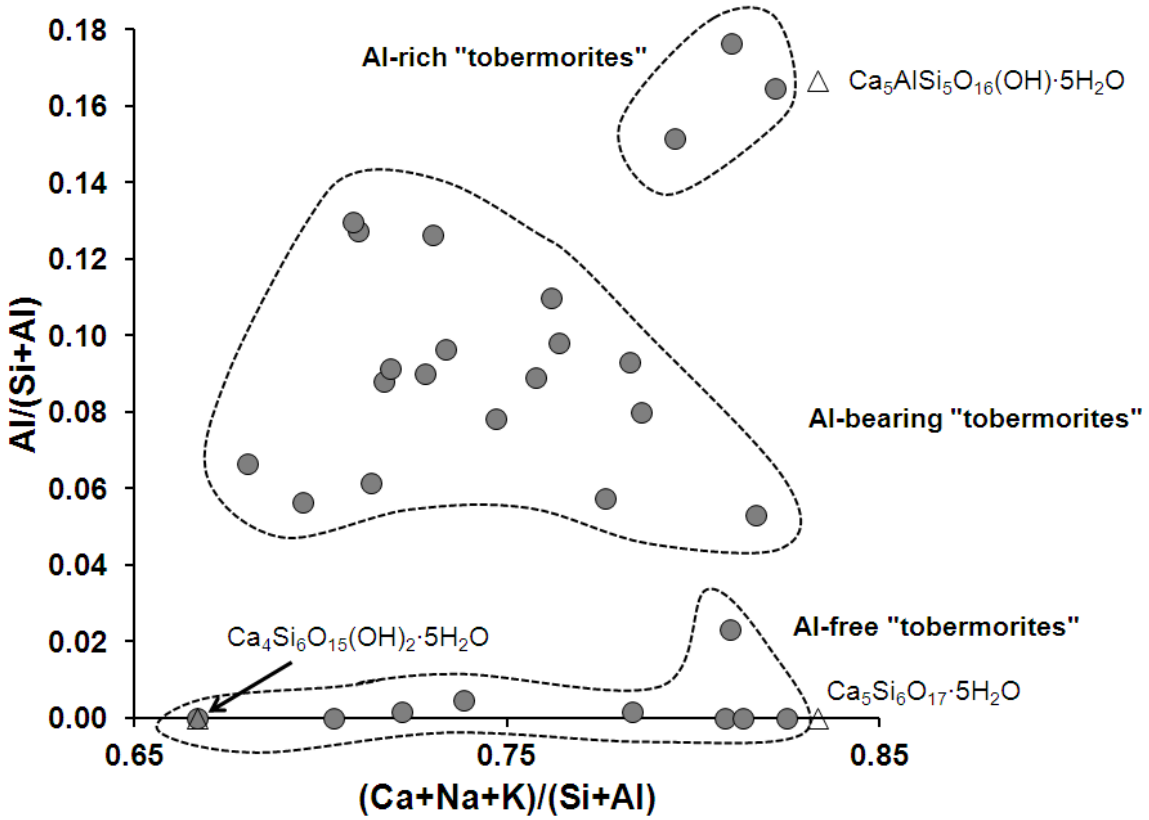

548

549

550

551

552 **Figure 3** – TG and DSC curves (dashed and solid line, respectively) for tobermorite from Montalto
553 di Castro (a) and Vallerano (b).

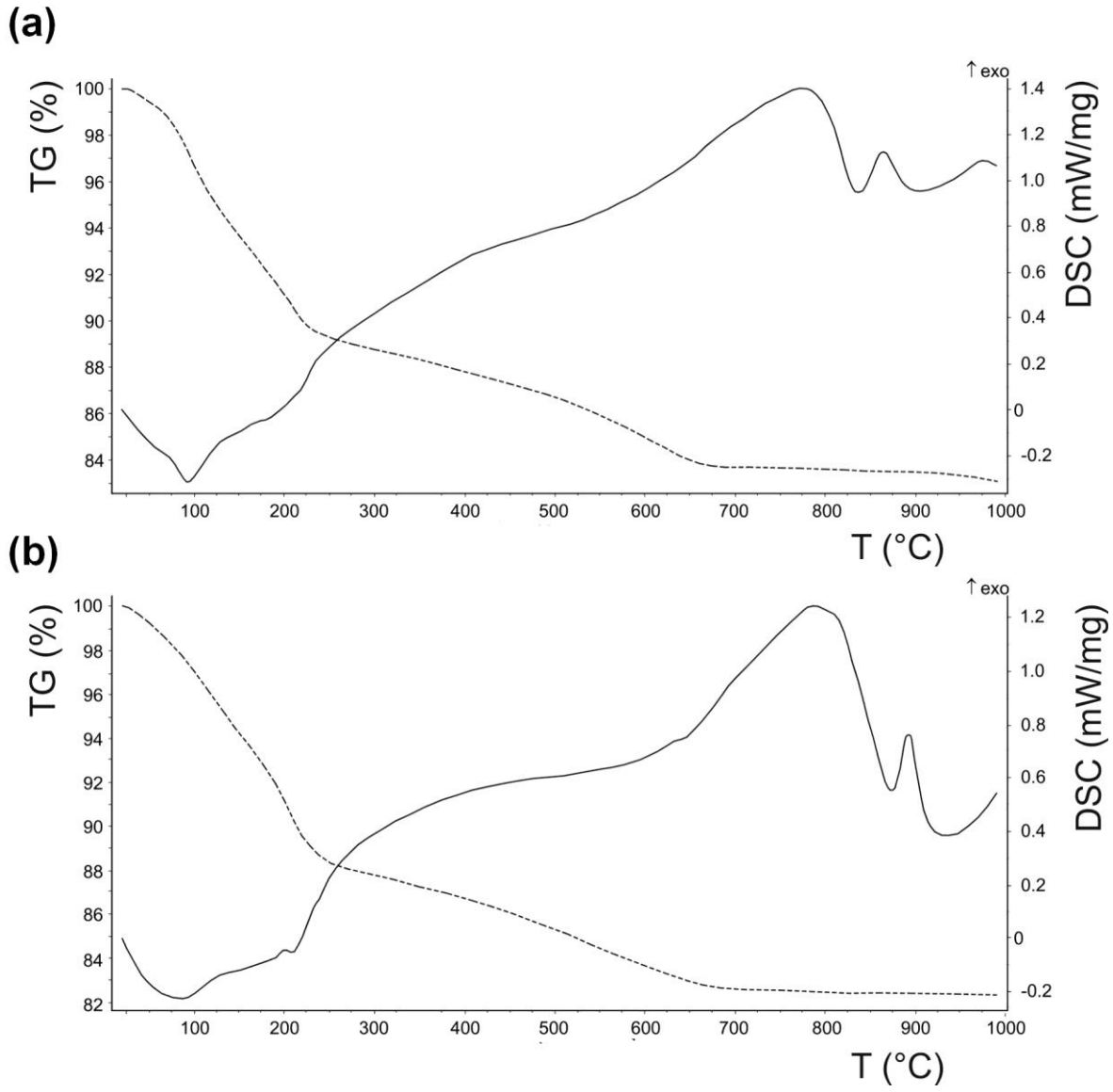

554

555

Figure 4 – X-ray powder diffraction patterns collected at the GILDA beamline upon heating. In (a) the 2θ range 3-45° is shown, whereas in the inset (b) it may be appreciated the disappearing of ettringite above 100°C and the occurrence of well crystallised "tobermorite 9Å" at 300°C.

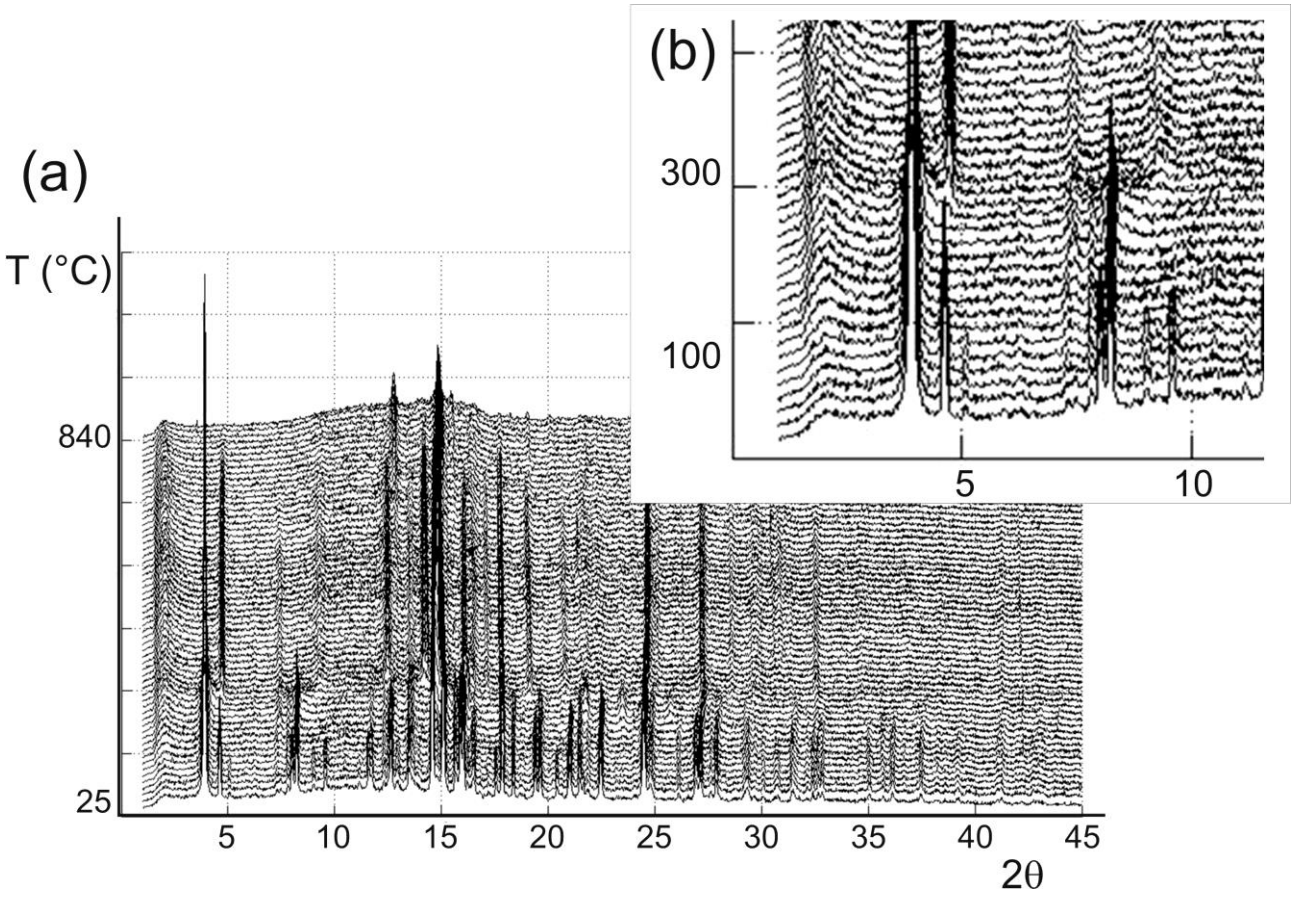

Figure 5 –The 2θ ranges (in °) described in the text showing the progressive disappearance of the X-ray diffraction effects related to tobermorite and the transient appearance of clinotobermorite. Diagnostic reflections are marked with their spacing d_{hkl} (in Å) and *hkl* indices.

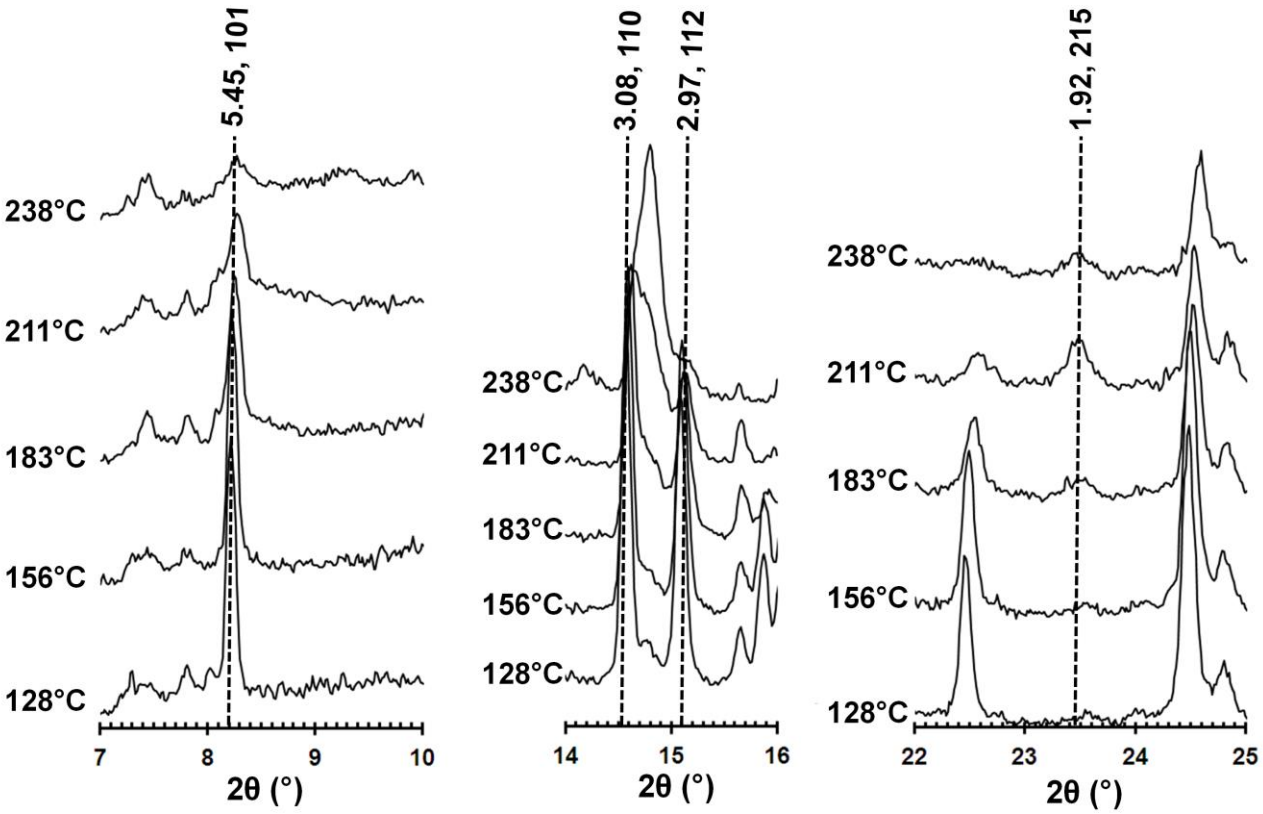

Figure 6 – Relative variations *R* of the unit-cell parameters (a) and unit-cell volume (b) for Al-rich tobermorite from room temperature up to its disappearance.

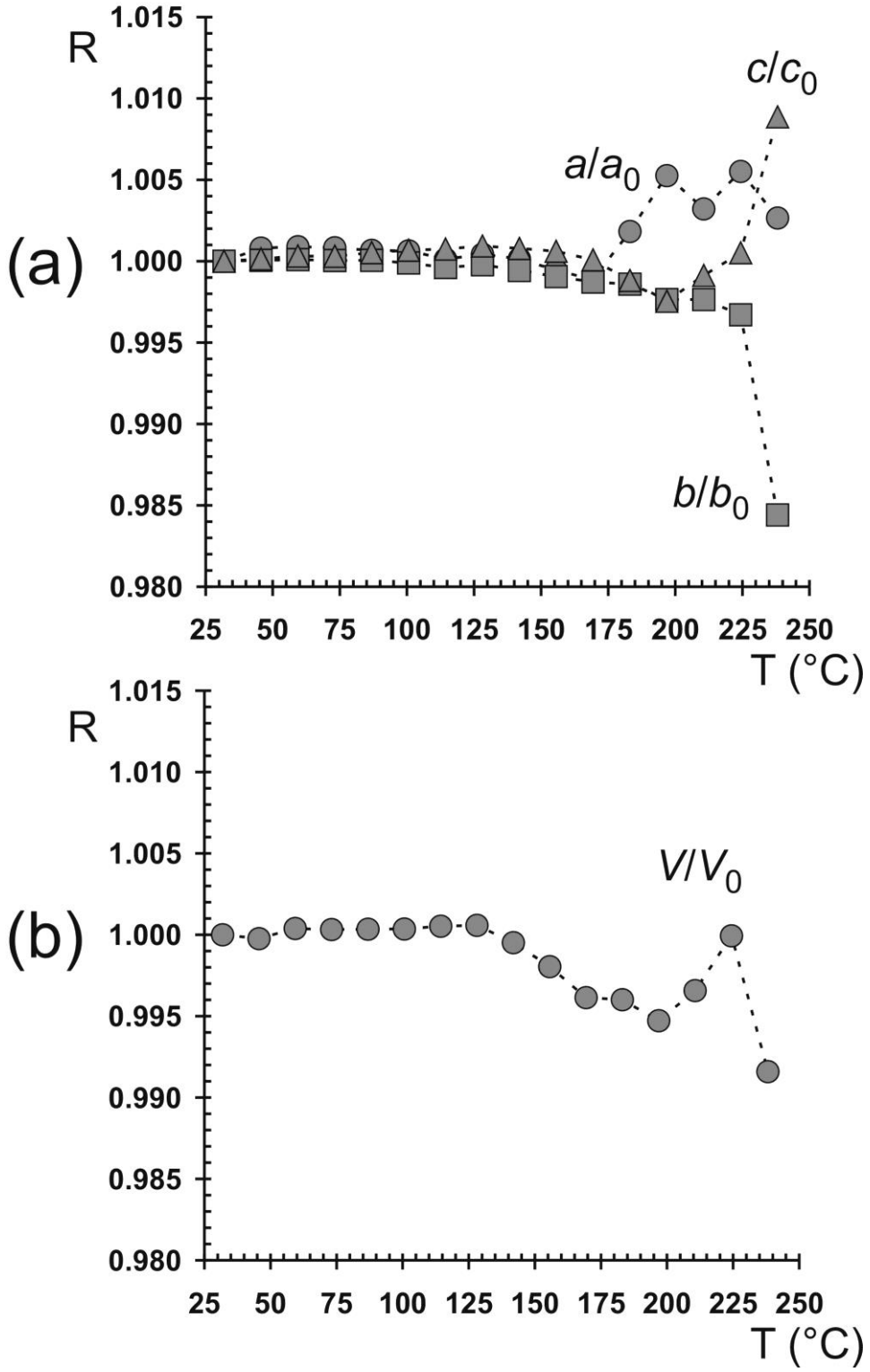

Figure 7 – The relative variation in the unit-cell parameter c (related to the basal spacing) in tobermorite and "tobermorite 9 Å" with respect to the unit-cell parameter c_0 of tobermorite at room temperature.

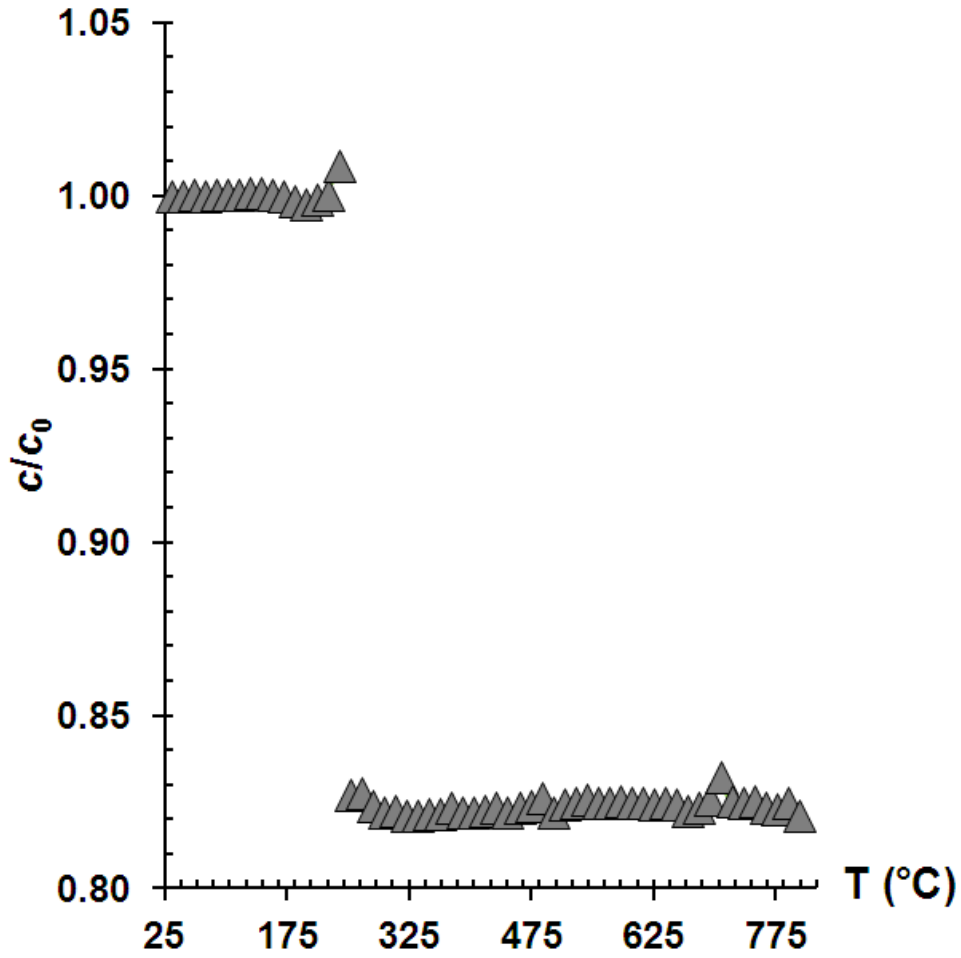

Figure 8 – The different conformation of silicate chains in tobermorite (a), clinotobermorite (b) and "tobermorite 9 Å" (c), as seen down [010]. Si-centered tetrahedra are drawn in black, whereas the Ca-centered polyhedra are grey. Circles are (in order of decreasing size) additional Ca cations and H_2O molecules.

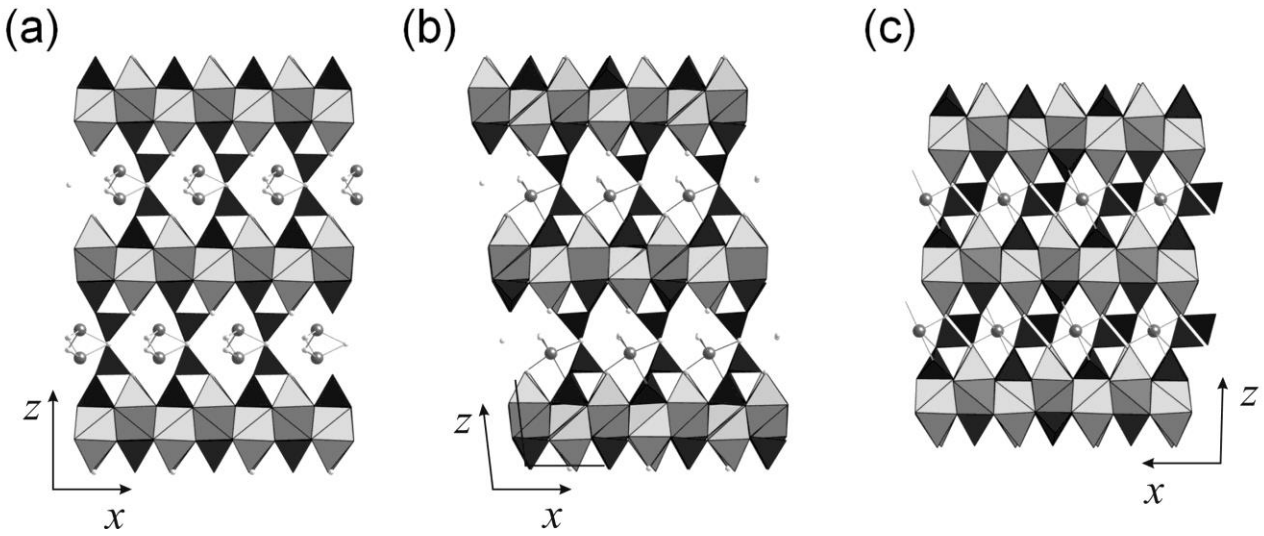

Figure captions

Figure 1 – Globular aggregates of thin platy crystals of tobermorite associated with calcite. Vallerano, Latium, Italy.

Figure 2 – Chemical variability in natural 11 Å members of the tobermorite supergroup.

Figure 3 – TG and DSC curves (dashed and solid line, respectively) for tobermorite from Montalto di Castro (a) and Vallerano (b).

Figure 4 – X-ray powder diffraction patterns collected at the GILDA beamline upon heating. Only the 2θ range 3-45° is shown.

Figure 5 – The 2θ ranges (in °) described in the text showing the progressive disappearance of the X-ray diffraction effects related to tobermorite and the transient appearance of clinotobermorite. Diagnostic reflections are marked with their spacing d_{hkl} (in Å) and *hkl* indices.

Figure 6 – Relative variations *R* of the unit-cell parameters (a) and unit-cell volume (b) for Al-rich tobermorite from room temperature up to its disappearance.

Figure 7 – The relative variation in the unit-cell parameter *c* (related to the basal spacing) in tobermorite and "tobermorite 9 Å" with respect to the unit-cell parameter c_0 of tobermorite at room temperature.

Figure 8 – The different conformation of silicate chains in tobermorite (a), clinotobermorite (b) and "tobermorite 9 Å" (c), as seen down [010]. Si-centered tetrahedra are drawn in black, whereas the Ca-centered polyhedra are grey. Circles are (in order of decreasing size) additional Ca cations and H_2O molecules.